

Development of Metal Oxide High-Pressure Phases for Photocatalytic Properties by Severe Plastic Deformation

Hadi Razavi-Khosroshahi and Masayoshi Fuji*

Advanced Ceramics Research Center, Nagoya Institute of Technology, Tajimi 507-0033, Japan

Photocatalytic activity of most metal oxides is restricted to the ultraviolet (UV) range of solar spectrum due to their large band gap. Since UV accounts for only 5% of the solar spectrum, designing metal oxide semiconductors with capability of absorbing visible light has been widely attempted. The large band gap of metal oxides can be reduced by various methods like doping with metallic or non-metallic ions, however a better photocatalytic activity can not be achieved necessarily by these methods due to fast recombinations of electron and hole. In recent years, authors have paid attention to the high pressure phases of metal oxides, which theoretically possess narrow band gaps, being able to absorb visible light. In this review, high pressure phases of well-known metal oxides like titania (TiO_2), zirconia (ZrO_2), and yttria (Y_2O_3) have been stabilized by applying a severe plastic deformation method, and photocatalytic properties of them have been evaluated.

[doi:10.2320/matertrans.MF201916]

(Received January 31, 2019; Accepted March 18, 2019; Published May 31, 2019)

Keywords: metal oxides, high-pressure torsion (HPT), titanium dioxide (titania), zinc oxide (zirconia), yttrium oxide (yttria)

1. Introduction

One of the major challenges in the last decades has been how to provide sufficient energy to the world's population. It is nowadays clear that fossil fuels, which currently supply about 85% of our necessary energy, will be unable to satisfy the increased energy demand in the future. Therefore, reducing the dependence of society on fossil fuels and a large-scale transition toward a new and sustainable source of energy is unavoidable. Among various sustainable energy sources such as wind, geothermal, biomass, and nuclear, solar energy has the best potential for meeting our energy needs.¹⁾ Saving sun energy in the form of hydrogen by splitting water into hydrogen and oxygen is one of the most attractive possibilities, which can occur in the presence of a photocatalyst.

Metal oxide semiconductors which are abundant in nature are considered as less expensive, biocompatible, and stable photocatalysts under various environments.²⁾ The application of metal oxide photocatalysts is decomposing organic pollutants in water/air, photovoltaics, and splitting water into hydrogen and oxygen. Despite their excellent features, the photocatalytic activity of most metal oxides is limited to the ultraviolet (UV) range of sunlight due to their large band gap.²⁾ Since UV accounts for only 5% of the solar spectrum, designing metal oxide semiconductors with the capability of absorbing visible light has been widely attempted. The large band gap of metal oxides can be reduced by methods like metal loading,³⁾ ion implantation,⁴⁾ and anion/cation doping,^{5,6)} however, such approaches do not necessarily lead to higher photocatalytic activity due to the defect-induced electron/hole recombination losses.^{7,8)}

Narrowing the band gap of pure metal oxide semiconductors has been extensively investigated in recent decades.^{9,10)} According to theoretical studies, high-pressure phases of metal oxides show narrower band gaps in the range of visible light.¹¹⁻¹⁵⁾ However, most of these high-pressure phases are not stable under ambient pressure and transform to

their stabler phases irreversibly upon decompression. High-pressure torsion (HPT) method^{16,17)} is known as an effective method for stabilization of high-pressure phases under room pressure. In this technique, high pressure and plastic strain are simultaneously induced to the material between two rotating anvils. The large plastic strain and lattice defect formation change the thermodynamic behavior of phases at ambient pressure. It is reported that high-pressure phases could be stabilized at ambient pressure in several materials: black phosphorous in P,¹⁶⁾ diamond-like phases in Carbon,¹⁸⁾ ω phase in Zirconium and Titanium,¹⁹⁾ cubic phase in barium titanate.²⁰⁾ Since there are very few reports on the high-pressure stabilization of metal oxides, the HPT method is employed for various metal oxides like TiO_2 , ZnO , and Y_2O_3 . In the following, each material will be reviewed in terms of high-pressure phases, phase transformations, optical and photocatalytic properties.

2. Results and Discussion

2.1 Titanium dioxide (TiO_2)

TiO_2 or titania was the first material described as a water-splitting photocatalyst as described first by Fujishima and Honda in 1971.²¹⁾ TiO_2 crystallizes in three types of polymorphs: Rutile with a band gap of 3.0 eV, Anatase with a band gap: 3.2 eV, and Brookite.²²⁾ High-pressure phases of TiO_2 have theoretically been calculated to have lower band gaps coinciding with the visible light. For example, columbite TiO_2 -II with a orthorhombic structure is shown to have a band gap of 2.59 eV.^{14,15)} However, TiO_2 -II is stable at pressures higher than 2 GPa according to the phase diagram.

The starting powder for HPT processing was pure anatase with an average particle size of 150 nm. Plastic strain was introduced under 1 and 6 GPa by rotating two anvils for 0, 1/16, 1/4, 1, and 4 turns and discs with 10 mm diameter and 0.8 mm thickness were obtained. Lattice defects were reduced by annealing the HPT-processed discs at 500°C. Phase transformations were confirmed by X-ray diffraction (XRD), and microstructures were observed by transmission

*Corresponding author, E-mail: fuji@nitech.ac.jp

electron microscopy. Band gap of each sample was calculated by UV-Vis diffuse reflectance spectroscopy. Photocatalytic hydrogen evolution was examined in a solution of 500 g TiO₂ sample, 25 cm³ methanol, 225 cm³ distilled water and 1.325 cm³ H₂PtCl₆·6H₂O under UV light and visible light.

XRD results for HPT samples under 1 and 6 GPa are shown in Fig. 1(a). A distinct peak broadening is confirmed for samples after HPT processing, indication of lattice strain and lattice defects.²³⁾ In addition to anatase, TiO₂-II is also confirmed for samples after HPT processing. It is important to notice that TiO₂-II phase is present below 1 GPa, which is lower than the reported pressure for TiO₂-II formation. This decrease in the critical pressure is considered to be due to the plastic strain effect.

The relation between plastic strain and phase transformation is shown in XRD results of Figs. 1(b) and (c). The intensity and the fraction of TiO₂-II increase with HPT turns. The relation between phase fraction increase and strain in Fig. 1(c) is comparable to those of HPT-processed metallic materials^{24,25)} and ceramics.^{26–30)}

Figure 2(a) shows the UV-Vis spectra of samples before HPT, after HPT and after annealing at 500°C.³¹⁾ While the absorption edge of starting powders is 400 nm, it shifts to the visible light region, 470 nm, after HPT. A blue shift of absorption edge after annealing is due to slight phase transformation of TiO₂-II to anatase.

The Band gap of all samples are calculated by the Kubelka-Munk equation as shown in Fig. 2(b), being 3.1, 2.4, and 2.7 eV for samples before HPT, after HPT and after annealing, respectively. Comparing the band gaps of starting powder and that of the annealed sample shows that the formation of columbite TiO₂-II effectively narrows down the band gap of TiO₂.

Finally, the rate of photocatalytic hydrogen generation by water splitting was examined. Photocatalytic hydrogen generation against reaction time under UV and visible lights are shown in Figs. 3(a) and 3(b), respectively. It is obvious that hydrogen production rate under is slower for the HPT sample under UV comparing with that for the starting sample. However, the water split rate is faster for the HPT sample under visible light. Water split rate both under UV and visible lights significantly enhances after annealing. It can be concluded that HPT process successfully stabilized the high-pressure TiO₂-II phase, and as a consequence band gap was reduced. This led to an efficient water split reaction under visible light.

Another feature that should be considered is grain size effect. Authors by examining 80 grains by high-resolution TEM noticed that nanograins with sizes less than 15 nm had a TiO₂-II structure, while larger grains had an anatase structure.

2.2 Zinc oxide (ZnO)

Zinc oxide (ZnO) has a wurtzite crystal structure in ambient pressure and temperature with the space group of P6₃mc. Wurtzite ZnO is known as a stable, non-toxic and cheap semiconductor with excellent photocatalytic features,³²⁾ finding its application as antibacterials, biochemical sensors, and photovoltaic cells. However, like TiO₂, a large band gap of 3.4 eV limits the photocatalytic application of pure ZnO to the UV range of sunlight. Although doping ZnO

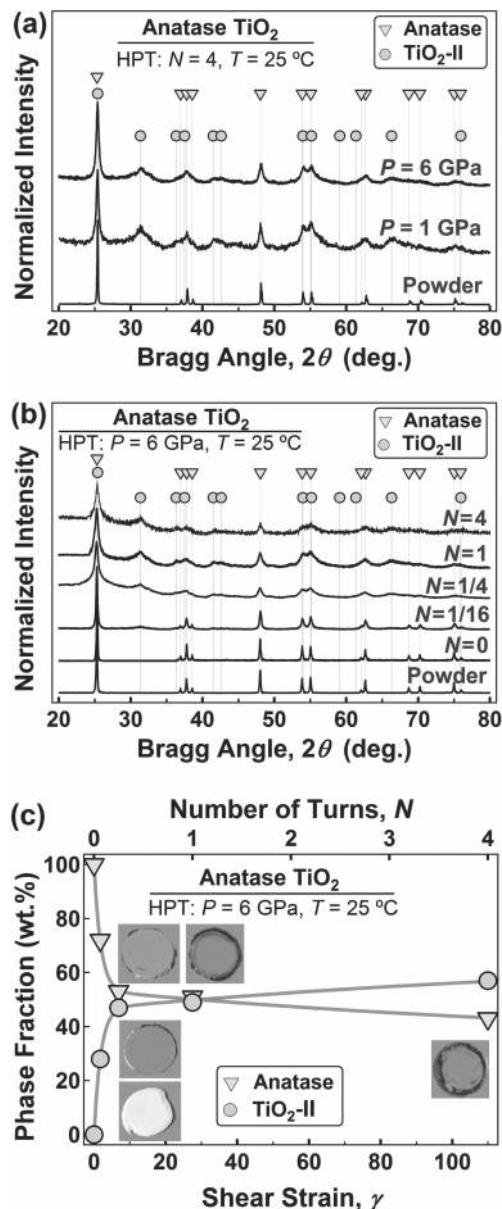


Fig. 1 (a) XRD profiles for raw powder and HPT processed samples at 1 and 6 GPa for 4 turns, (b) XRD profiles after HPT under 6 GPa for different turns, and (c) Rietveld analysis results.²³⁾

with cations or anions can reduce the band gap of ZnO, there are also some limitations in this regard.³³⁾ In ZnO, dopants tend to precipitate and change the chemical composition of the host. Another limitation is the solubility of dopants in ZnO, which are usually very low. Since high temperatures are usually required for enhancing the crystallinity of ZnO, undesired expulsion of dopant can occur easily. Also, under rigorous pH changes dopants usually leach from the host ZnO.

Wurtzite ZnO can transform to high-pressure rocksalt phase under high pressures as shown in Fig. 4(a).³⁴⁾ Theoretical studies on ZnO^{35,36)} have proved that the band gap of the rocksalt phase is in the range of 1.2–2.6 eV. However, the wurtzite phase is the only stable phase of ZnO at the ambient pressure, while the rocksalt phase can only exist at pressures higher than 6–10 GPa. Recently, authors have successfully stabilized rocksalt phase with a large

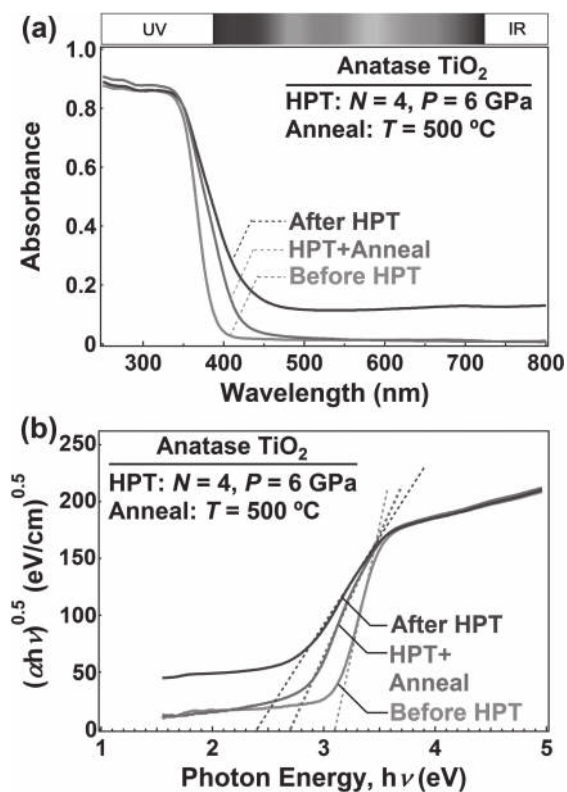


Fig. 2 (a) UV-Vis profiles, and (b) band gap calculation of TiO_2 .³¹⁾

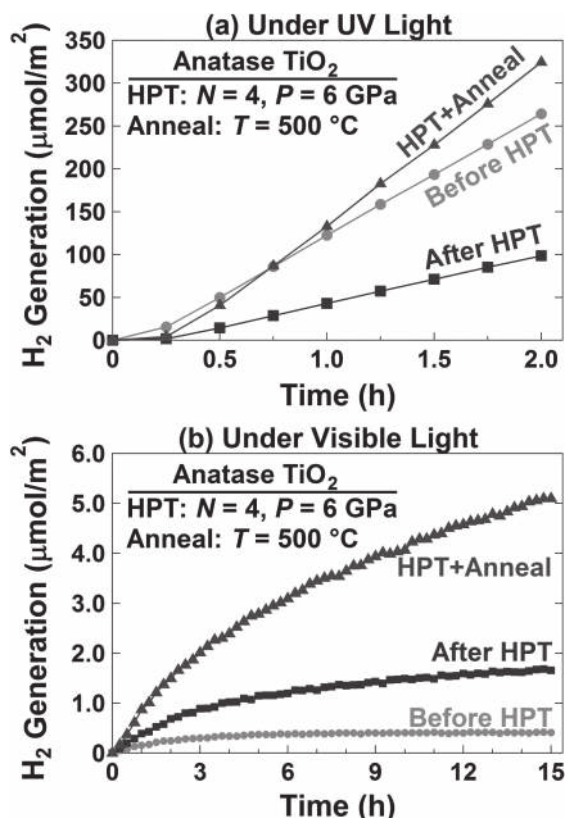


Fig. 3 Photocatalytic water splitting test of TiO_2 under (a) UV light and (b) visible light.³¹⁾

fraction of oxygen vacancies by HPT method, as schematically shown in Fig. 4(b). The photocatalytic activity of the rocksalt phase is also examined for the first time.³⁷⁾

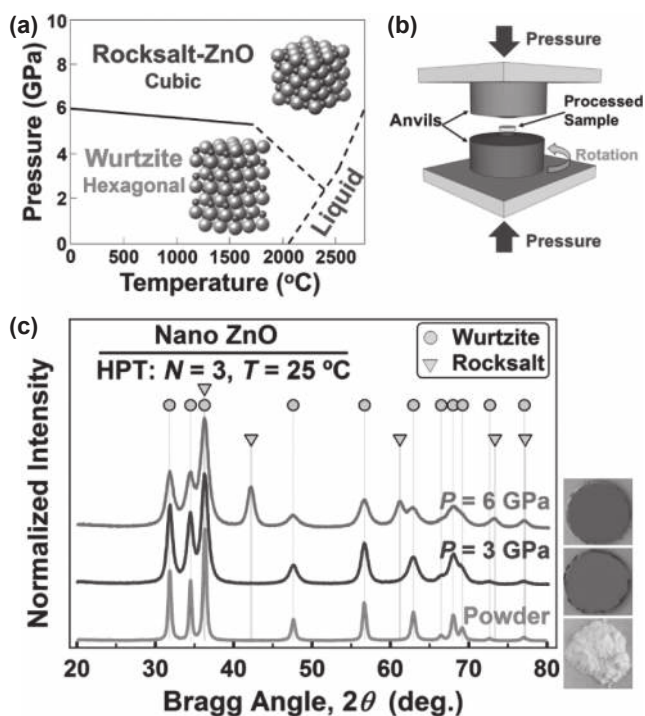


Fig. 4 (a) Phase diagram of ZnO, (b) HPT device, (c) XRD profiles after HPT.³⁷⁾

The crystal structure of wurtzite starting powder and HPT processed samples under 3 and 6 GPa are examined by XRD, as shown in Fig. 4(c). In addition to wurtzite peaks in the powder and in the samples after HPT, a distinct peak broadening after HPT processing was confirmed due to the lattice strain and grain size reduction with an average grain size of 11 nm. Also, rocksalt phase with a fraction of 50 wt.% could be confirmed for the HPT sample under 6 GPa. The rocksalt phase formation, suggested that simultaneous introduction of pressure and strain is vital for stabilization of the rocksalt phase under ambient pressure. In this study, a correlation between grain size and crystal structure could not be confirmed for ZnO due to the unstable feature of the rocksalt phase under electron beam irradiation. In addition, the color of samples changed from white to dark yellow after HPT processing due to the formation of oxygen vacancies.

Figure 5(a) shows the UV-Vis profile of the starting ZnO powder, HPT sample under 3 GPa, and 6 GPa. ZnO powder showed an absorption edge at 400 nm, while it redshifted to the visible light area with absorption edge of 460 and 650 nm for the samples processed at 3 and 6 GPa, respectively. Band gaps were calculated from the UV-Vis as shown in Fig. 5(b), being 3.1, 2.8, and 1.8 eV for the starting powder and for the samples processed at 3 and 6 GPa. Band gap narrowing of sample processed at 3 GPa is due to the introduction of oxygen vacancies. Oxygen vacancies are known to create energy states above the valance band, leading to band gap reduction of ZnO. However, a large band gap reduction of sample at 6 GPa is anomalous and cannot be explained only by the presence of oxygen vacancies. This band gap reduction is attributed to the formation of rocksalt phase. The photocatalytic activity of samples was examined by measuring the degradation rate of Rhodamine B (RhB) under visible light and results are shown in Fig. 5(c). On one hand,

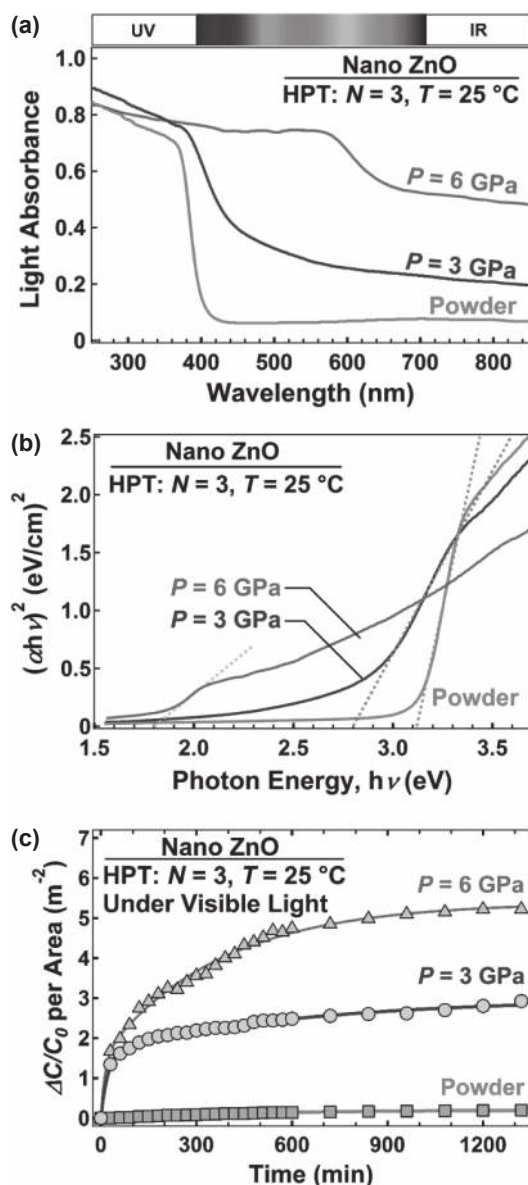


Fig. 5 (a) UV-Vis profiles of ZnO before and after HPT, (b) band gap calculation, (c) photocatalytic activity under visible light.³⁷⁾

wurtzite powder shows little RhB degradation, and on the other hand, the sample processed at 3 GPa exhibits higher photocatalytic activity due to the formation of oxygen vacancies. The HPT sample at 6 GPa shows even better activity due to the rocksalt phase formation with a band gap of 1.8 eV. It is clear from these results that HPT could successfully stabilize the rocksalt phase of ZnO with a band gap as narrow as 1.8 eV, which was able to absorb the visible light extensively.

2.3 Yttrium oxide (Y₂O₃)

In this part, high-pressure phase stabilization and band gap reducing of Y₂O₃, as well as its optical properties, will be introduced. Y₂O₃ is an insulator ceramic with the high melting point, superior mechanical properties, and good chemical stability.³⁸⁾ Y₂O₃ doped with rare earth elements is widely used as phosphor materials, lasers, bioimaging, fluorescent lamps, and field emission displays thanks to its optical properties.

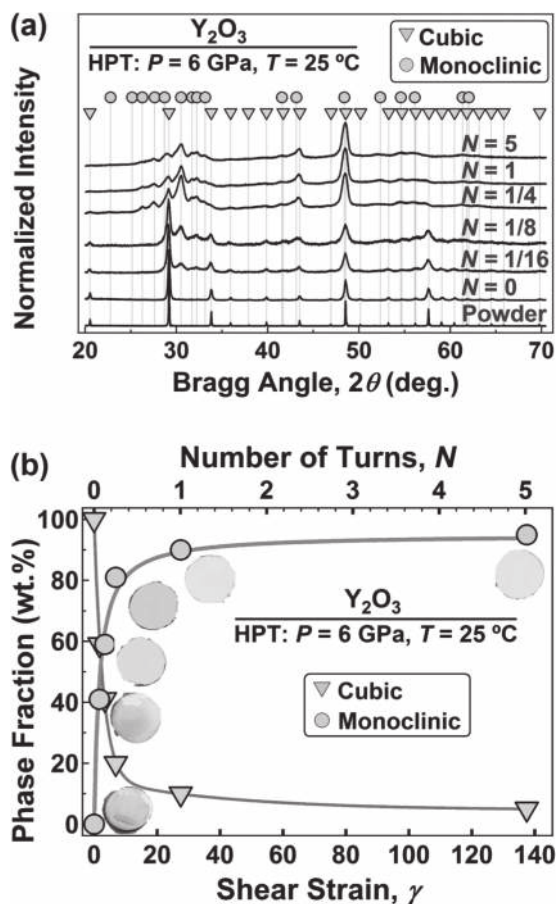


Fig. 6 (a) XRD results for Y₂O₃ before and after HPT, (b) Rietveld analysis results.⁴⁰⁾

According to the pressure-temperature phase diagram, Y₂O₃ has a cubic structure at ambient pressure and transforms into the monoclinic and hexagonal phases as pressure increases.³⁹⁾ However, since these high-pressure phases are unstable at ambient pressure upon decompression, the HPT method may stabilize these phases, inspired by previous works on TiO₂ and ZnO. It is reported that monoclinic Y₂O₃ show better PL intensities than that of the cubic phase, therefore its stabilization at ambient pressure is extremely meaningful.

XRD profiles of samples processed by HPT at 6 GPa are shown in Fig. 6(a).⁴⁰⁾ Again, a peak broadening due to lattice strain and grain size reduction is confirmed during the process. Peak broadening was not distinct by pure compression ($N = 0$), while became more distinct by rotating the anvils, revealing that the plastic strain could be successfully introduced to the hard and brittle Y₂O₃. Also, mere compression only leads to cubic phase, while the monoclinic phase appears after HPT processing. In addition, the fraction of monoclinic phase increased with increasing the plastic strain and reached 90%. Rietveld analysis results are shown in Fig. 6(b). The color of the samples also changed from white to dark pink by HPT processing not due to the monoclinic phase formation, but due to the particle size reduction of Y₂O₃ nanometer level.

Figure 7 shows the photoluminescence (PL) profile of starting powder and samples processed by HPT under 6 GPa with different turn numbers. In Y₂O₃ with Eu impurities, four

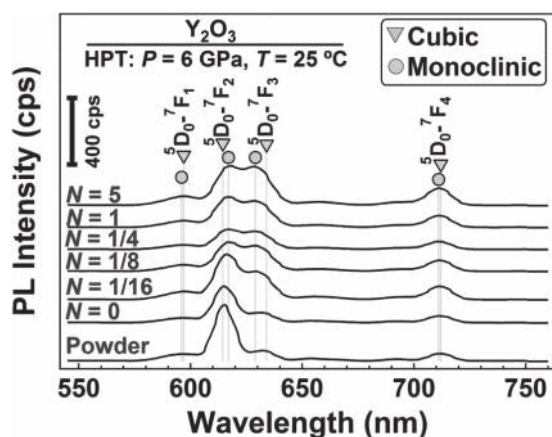


Fig. 7 PL spectra profiles for Y_2O_3 before and after HPT process.⁴⁰⁾

PL transitions are allowed: $^5D_0 \rightarrow ^7F_J$ ($J = 1, 2, 3, 4$).⁴¹⁾ The $^5D_0 \rightarrow ^7F_1$ transition is centrosymmetric, while three other transitions are non-centrosymmetric. It is shown that as the turn numbers of HPT increase, the intensity of $^5D_0 \rightarrow ^7F_2$ decreases, and the $^5D_0 \rightarrow ^7F_3$ intensity increases. Since the $^5D_0 \rightarrow ^7F_2$ transition has the character of electric dipole, and the $^5D_0 \rightarrow ^7F_3$ transition is mainly magnetic dipole, it can be concluded that the PL characteristic changes from the electric dipole to magnetic dipole by the formation of monoclinic phase. In addition, $4f$ electrons are known to be shielded by outer electrons like $5s^2$ and $5p^6$, they are extremely sensitive to the surrounding lattice structure.⁴²⁾ To this reason, the cubic-to-monoclinic transition changes the Y_2O_3 electric field strength and a new peak at 629 nm forms. It is important to note that, although the grain size and crystallinity of Y_2O_3 are significantly reduced by HPT, PL intensity is almost the same. Materials with better crystallinity and larger particles show higher PL intensity, while nanomaterials show poor PL features because quench sites for photo-excited electrons are abundant on the free surfaces and grain boundaries.

Finally, the effect of grain size on the phase transformation was studied by Examining of 150 grains using TEM. Results showed that grains smaller than 22 nm had a monoclinic structure, while larger grains had a cubic structure, indicating the important role of grain size on the phase formation and stability.

2.4 Effect of strain on critical pressure reduction for phase transformations and its mechanism

Phase transformations of each metal oxide under hydrostatic pressure, and under HPT is summarized as follows:

- (I) Under hydrostatic pressure, anatase TiO_2 transforms to the columbite TiO_2 -II at 2.5–7 GPa.^{43–46)} Under HPT, the minimum pressure required for the phase transformation was 1 GPa.
- (II) Under hydrostatic pressure, wurtzite ZnO transforms to the rocksalt ZnO at pressures over 6–10 GPa.⁴⁷⁾ Under HPT, the minimum pressure required for the phase transformation was 6 GPa.
- (III) Under hydrostatic pressure, cubic Y_2O_3 transforms to the monoclinic Y_2O_3 at 12–15 GPa.^{48–50)} Under HPT, the minimum pressure required for the phase transformation was 6 GPa.

Microstructural analyses proved that the stability of high-pressure phases at ambient pressure was due to the grain size effect, in good agreement with the earlier reports in HPT-processed metals and metal oxides.^{19,20,51)} The formation of high-pressure phases below the critical pressure, clearly proved the critical role of strain on overcoming the energy barrier for high-pressure phase nucleations. In mere compression, high-pressure phases nucleate at lattice defects such as dislocations that are already present within the material.⁵²⁾ Since the fraction of these defects is usually low, high pressures are required to overcome the energy barrier for nucleation. In HPT, however, a large number of new defects continuously generate by plastic deformation.⁵³⁾ Therefore, nucleation sites are abundant and thus the pressure required for phase transformation becomes lower. The pile-up of lattice defects such as dislocations at grain boundaries also provides an effective pressure tensor concentrator, which can reduce the threshold for phase transformation.

3. Conclusions

In this review, the effect of plastic strain on the phase transformation and defect engineering of well-known metal oxides like TiO_2 , ZnO, and Y_2O_3 were summarized. Severe plastic deformation was applied to all materials by a high-pressure torsion (HPT) method, and high-pressure phases were stabilized at ambient pressure. Furthermore, the effect of phase transformation on photocatalytic and optical properties were investigated.

- (1) Anatase TiO_2 transformed to columbite TiO_2 -II phase, and the band gap reduced from 3.1 eV to 2.4 eV. Photocatalytic water split test under visible light showed that the high-pressure phase stabilized by HPT was able to split water successfully, while anatase did not show any activity.
- (2) Wurtzite ZnO transformed to rocksalt ZnO by HPT and remained stable at ambient pressure. The band gap reduced from 3.1 eV to 1.8 eV and photocatalytic activity under visible light improved extensively.
- (3) Cubic Y_2O_3 transformed to monoclinic Y_2O_3 by HPT and remained stable at room pressure. Comparing PL profile of samples before and after HPT showed that a new peak at 629 nm formed after HPT processing, indicating the change of PL characteristic from electric dipole to magnetic dipole.
- (4) While a critical grain size for phase transformation was confirmed for TiO_2 and Y_2O_3 , this correlation was not confirmed for ZnO.

Acknowledgments

This work was supported, in part, by JST A-STEP Grant Number JPMJTS1621, Japan.

REFERENCES

- 1) N.S. Lewis and D.G. Nocera: *Proc. Natl. Acad. Sci. USA* **103** (2006) 15729–15735.
- 2) S. Martha, P.C. Sahoo and K.M. Parida: *RSC Adv.* **5** (2015) 61535–61553.
- 3) I. Robel, V. Subramanian, M. Kuno and P.V. Kamat: *J. Am. Chem. Soc.*

- 128** (2006) 2385–2393.
- 4) O. Diwald, T.L. Thompson, E.G. Goralski, S.D. Walck and J.T. Yates: *J. Phys. Chem. B* **108** (2004) 52–57.
 - 5) H. Irie, Y. Watanabe and K. Hashimoto: *Chem. Lett.* **32** (2003) 772–773.
 - 6) R. Asahi, T. Ohwaki, K. Aoki and Y. Taga: *Science* **293** (2001) 269–271.
 - 7) W.Y. Choi, A. Termin and M.R. Hoffmann: *J. Phys. Chem.* **98** (1994) 13669–13679.
 - 8) G. Zhao, H. Kozuka, H. Lin, M. Takahashi and T. Yoko: *Thin Solid Films* **340** (1999) 125–131.
 - 9) X. Chen, L. Liu, P.Y. Yu and S.S. Mao: *Science* **331** (2011) 746–750.
 - 10) J. Tao, T. Luttrell and M. Batzill: *Nat. Chem.* **3** (2011) 296–300.
 - 11) M. Mattesini, J. de Almeida, L. Dubrovinsky, N. Dubrovinskaia, B. Johansson and R. Ahuja: *Phys. Rev. B* **70** (2004) 115101.
 - 12) M.Y. Kuo, C.L. Chen, C.Y. Hua, H.C. Yang and P. Shen: *J. Phys. Chem. B* **109** (2005) 8693–8700.
 - 13) M. Niu, D. Cheng and D. Cao: *J. Phys. Chem. C* **118** (2014) 20107–20111.
 - 14) T. Zhu and S.-P. Gao: *J. Phys. Chem. C* **118** (2014) 11385–11396.
 - 15) W.-N. Zhao, S.-C. Zhu, Y.-F. Li and Z.-P. Liu: *Chem. Sci.* **6** (2015) 3483–3494.
 - 16) P.W. Bridgman: *Phys. Rev.* **48** (1935) 825–847.
 - 17) R.Z. Valiev, Y. Estrin, Z. Horita, T.G. Langdon, M.J. Zehetbauer and Y.T. Zhu: *JOM* **58** (2006) 33–39.
 - 18) K. Edalati, T. Daio, Y. Ikoma, M. Arita and Z. Horita: *Appl. Phys. Lett.* **103** (2013) 034108.
 - 19) K. Edalati, T. Daio, M. Arita, S. Lee, Z. Horita, A. Togo and I. Tanaka: *Acta Mater.* **68** (2014) 207–213.
 - 20) K. Edalati, M. Arimura, Y. Ikoma, T. Daio, M. Miyata, D.J. Smith and Z. Horita: *Mater. Res. Lett.* **3** (2015) 216–221.
 - 21) A. Fujishima and K. Honda: *Nature* **238** (1972) 37–38.
 - 22) K. Rajeshwar, N.R. de Tacconi and C.R. Chenthamarakshan: *Chem. Mater.* **13** (2001) 2765–2782.
 - 23) H. Razavi-Khosroshahi, K. Edalati, M. Arita, Z. Horita and M. Fujii: *Scr. Mater.* **124** (2016) 59–62.
 - 24) A.P. Zhilyaev and T.G. Langdon: *Prog. Mater. Sci.* **53** (2008) 893–979.
 - 25) R. Pippan, S. Scheriau, A. Taylor, M. Hafok, A. Hohenwarter and A. Bachmaier: *Annu. Rev. Mater. Res.* **40** (2010) 319–343.
 - 26) A.P. Zhilyaev, I. Sabirov, G. Gonzales-Doncel, J. Molina-Aldarequia, B. Srinivasarao and M.T. Perez-Prado: *Mater. Sci. Eng. A* **528** (2011) 3496–3505.
 - 27) N.Q. Chinh, R.Z. Valiev, X. Sauvage, G. Varga, K. Havancsak, M. Kawasaki, B.B. Straumal and T.G. Langdon: *Adv. Eng. Mater.* **16** (2014) 1000–1009.
 - 28) K. Edalati and Z. Horita: *Mater. Sci. Eng. A* **652** (2016) 325–352.
 - 29) K. Edalati, S. Toh, Y. Ikoma and Z. Horita: *Scr. Mater.* **65** (2011) 974–977.
 - 30) V.I. Levitas, Y. Ma, E. Selvi, J. Wu and J.A. Patten: *Phys. Rev. B* **85** (2012) 054114.
 - 31) H. Razavi-Khosroshahi, K. Edalati, M. Hirayama, H. Emami, M. Arita, M. Yamauchi, H. Hagiwara, S. Ida, T. Ishihara, E. Akiba, Z. Horita and M. Fujii: *ACS Catalysis* **6** (2016) 5103–5107.
 - 32) T. Takaki, K. Kurosawa, H. Razavi-Khosroshahi, S. Sukenaga, N. Saito, K. Kaneko, K. Nakashima and T. Hiraaki: *J. Am. Ceram. Soc.* **93** (2010) 3088–3091.
 - 33) S.G. Kumar and K.S.R.K. Rao: *RSC Adv.* **5** (2015) 3306–3351.
 - 34) L. Bayarjargal and B. Winkler: *Appl. Phys. Lett.* **100** (2012) 021909.
 - 35) A. Segura, J.A. Sans, F.J. Manjón, A. Muñoz and M.J. Herrera-Cabrera: *Appl. Phys. Lett.* **83** (2003) 278–280.
 - 36) A. Alvarado, J. Attapattu, Y. Zhang and C. Chen: *J. Appl. Phys.* **118** (2015) 165101.
 - 37) H. Razavi-Khosroshahi, K. Edalati, J. Wu, Y. Nakashima, M. Arita, Y. Ikoma, M. Sadakiyo, Y. Inagaki, A. Staykov, M. Yamauchi, Z. Horita and M. Fujii: *J. Mater. Chem. A* **5** (2017) 20298–20303.
 - 38) H. Razavi-Khosroshahi, H. Ikeda, K. Yamada, N. Saito, K. Kaneko, K. Hayashi and K. Nakashima: *J. Am. Ceram. Soc.* **95** (2012) 3263–3269.
 - 39) P.P. Bose, M.K. Gupta, R. Mittal, S. Rols, S.N. Achary, A.K. Tyagi and S.L. Chaplot: *Phys. Rev. B* **84** (2011) 094301.
 - 40) H. Razavi-Khosroshahi, K. Edalati, H. Emami, E. Akiba, Z. Horita and M. Fujii: *Inorg. Chem.* **56** (2017) 2576–2580.
 - 41) H. Forest and G. Ban: *J. Electrochem. Soc.* **116** (1969) 474–478.
 - 42) S. Ram and S.K. Sinha: *J. Solid State Chem.* **66** (1987) 225–234.
 - 43) F. Dacheville, P.Y. Simons and R. Roy: *Am. Mineral.* **53** (1968) 1929–1939.
 - 44) T. Ohsaka, S. Yamaoka and O. Shimomura: *Solid State Commun.* **30** (1979) 345–347.
 - 45) K. Lagarec and S. Desgreniers: *Solid State Commun.* **94** (1995) 519–524.
 - 46) T. Arlt, M. Bermejo, M.A. Blanco, L. Gerward, J. Jiang, J.S. Olsen and J.M. Recio: *Phys. Rev. B* **61** (2000) 14414–14419.
 - 47) L. Bayarjargal and B. Winkler: *Appl. Phys. Lett.* **100** (2012) 021909.
 - 48) J. Zhang, H. Cui, P. Zhu, C. Ma, X. Wu, H. Zhu, Y. Ma and Q. Cui: *J. Appl. Phys.* **115** (2014) 023502.
 - 49) E. Husson, C. Proust, P. Gillet and J.P. Itie: *Mater. Res. Bull.* **34** (1999) 2085–2092.
 - 50) H. Yusa, T. Tsuchiya, N. Sata and Y. Ohishi: *Inorg. Chem.* **49** (2010) 4478–4485.
 - 51) K. Edalati, S. Toh, M. Arita, M. Watanabe and Z. Horita: *Appl. Phys. Lett.* **102** (2013) 181902.
 - 52) V.I. Levitas: *Phys. Rev. B* **70** (2004) 184118.
 - 53) V.I. Levitas and M. Javanbakht: *Nanoscale* **6** (2014) 162–166.